Pergamon

Chemical Engineering Science, Vol. 49, No. 22, pp. 3791–3801, 1994

0009–2509/94 $7.00 + 0.00

0009–2509(94)00177–4

FLUOROPTIC MEASUREMENTS OF THE LOCAL HEAT TRANSFER COEFFICIENT INSIDE THE ROTATING CONE REACTOR

B. M. WAGENAAR, J. A. M. KUIPERS and W. P. M. VAN SWAAIJ
Department of Chemical Engineering, Twente University of Technology, PO Box 217, 7500 AE Enschede, The Netherlands

(*First received* 20 *October* 1993; *accepted in revised form* 17 *May* 1994)

Abstract—The rotating cone reactor is a novel reactor type for rapid thermal processing of solids. This paper focuses on the experimental determination of the gas-to-particle heat transfer coefficient. This quantity has been measured for several particle diameters (average size of 150, 280 and 425 μm) and cone rotational frequencies (11.3 and 28.3 Hz). The gas-to-particle heat transfer coefficient obtained from these experiments varied between 280 and 1030 $W m^{-2} K^{-1}$. Experimental parameters which were kept constant in this study were the particle mass flow rate (5 $g s^{-1}$), the cone geometry (cone top angle $\pi/3$ radians) and the temperature of the particle feed (280°C). The experimentally determined heat transfer coefficients were represented in dimensionless form as a function of the particle Reynolds number. The particle Reynolds number has been obtained from measurements of the local gas-phase velocity and the local particle velocity. Analysis of the experimental results revealed that the gas-to-particle heat transfer coefficients could roughly be represented by the well-established Ranz–Marshall correlation (Ranz and Marshall, 1952, *Chem. Engng Progress* **48**, 173) for isolated non-rotating particles. The difference between the experimentally observed particle Nusselt numbers and the theoretically predicted Nusselt numbers based on the Ranz–Marshall equation is probably due to the influence of particle rotation on the gas-to-particle heat transfer process. Calculations showed that the time in which the particles lose half of their rotation frequency is typically in the order of the particle residence time in the rotating cone reactor.

1. INTRODUCTION

The rotating cone reactor is a novel reactor type which can be used for rapid thermal processing of solids. A schematic representation of the rotating cone reactor geometry is presented in Fig. 1. Particles are introduced in the bottom of the rotating cone. The rotation of the cone induces particle motion and the particles are swept out of the reactor along a spiral path.

The rotating cone reactor has a number of desirable features, among which the most important ones are the following:

(1) A short particle residence time, typically 0.2 s. This short solids residence time is important in chemical systems in which the solids rapidly deactivate or rapidly react.

(2) Rapid heating of small particles, typically 5000 K/s. This rapid heating of particles is necessary if thermal processing of the solids is required (within the short solids residence time).

(3) Carrier gas is not required which is advantageous in systems where product dilution with the carrier gas has to be avoided.

A study concerning the particle dynamics and gas-phase hydrodynamics has been reported by Wagenaar *et al.* (1994a) in which the existence of a bouncing particle flow has been established under dilute flow conditions. This paper focuses on the transfer of heat to moving particles under similar dilute flow conditions, to obtain understanding with respect to the relevant transport phenomena influencing the performance of the rotating cone reactor.

The gas-to-particle heat transfer coefficient, α_p, is defined as the proportionality constant between the thermal driving force for the heat transfer (difference between gas and particle temperature) and the gas-to-particle heat flux:

$$Q_p'' = \alpha_p(T_p - T_g). \quad (1)$$

Simultaneous measurement of the thermal driving force and the corresponding heat flow rate to the particles enables the experimental determination of the apparent gas-to-particle heat transfer coefficient.

The thermal driving force $(T_p - T_g)$ has been obtained from the thermocouple measurement of the local gas-phase temperature, supplemented with measurements of the local particle temperature. This local particle temperature has been measured with a fluoroptic technique described elsewhere in more detail (Wagenaar *et al.*, 1994b).

The heat flow rate to the particles can be obtained from the measurements of the particle temperature at two distinct positions on a particle streamline. This heat flow rate to a particle is then equal to the ratio of the particle thermal energy difference and elapsed particle travelling time between the two points. In systems in which the particle thermal energy content only depends on temperature, the particle thermal

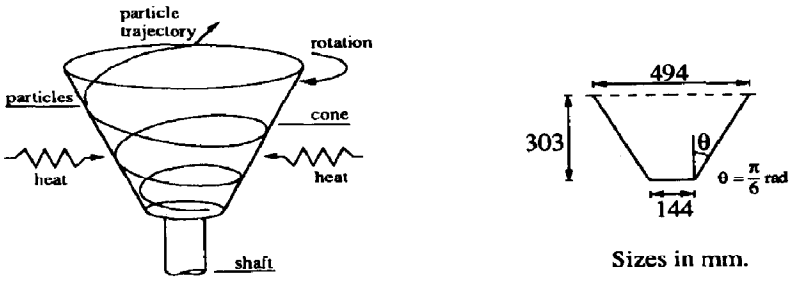

Fig. 1. Representation of the reactor principle and the cone geometry.

energy can be derived from a measurement of the local particle temperature. The elapsed time between the two points on a particle streamline is reciprocal to the local particle velocity. A combination of the local particle temperature and local particle velocity measurements yields the required information to quantify the heat flow rate to the particles. Each local particle velocity measurement has been performed under exactly the same conditions as the local particle temperature measurements.

Experimental results of Ranz and Marshall (1952) showed that the gas-to-particle heat transfer coefficient is dependent on the slip velocity between the particles and the gas phase. They obtained a good correlation between the dimensionless form of the gas-to-particle heat transfer coefficient (particle Nusselt number) and the dimensionless slip velocity (particle Reynolds number). Measurement of the particle slip velocity provides a valuable tool for interpretation of the gas-to-particle heat transfer rates.

2. EQUIPMENT AND EXPERIMENTAL PROCEDURES

The local particle velocity and the local particle temperature have been measured in a cold flow rotating cone using experimental techniques which have been described in more detail elsewhere (Wagenaar *et al.*, 1994a, b). This cone can be characterised by a top angle of $\pi/3$ radians and a maximum diameter of 494 mm. In the bottom of the cone a 144 mm diameter impeller has been mounted which releases particles with an angular velocity equal to the cone rotational speed. For experimental convenience, it was decided in the present heat transfer study to measure the cooling rate of the particles instead of the heating rate. Fluorescent particles with an initial temperature of 280°C were used to perform the cooling experiments. In all experiments the mass flow rate of the particles was 5 g s^{-1}, which corresponds to a solids volume fraction of 4×10^{-5} (for particles with a bouncing height of 15 mm). Particle physical properties are listed in Table 1. All parts of the cold flow facility had a well-defined constant temperature (i.e. approximately room temperature). This isothermal condition could be maintained during the experiments because the heat capacity of the fluorescent particles was small compared to the heat capacity of the gas phase inside the rotating cone reactor. The geometry of the cone is presented in Fig. 1. A schematic representation of the cold flow facility is given in Fig. 2.

Table 1. Particle physical properties

Density ρ_p	6000 kg m^{-3}
Heat capacity C_p	318 J kg^{-1} K^{-1}
Thermal conductivity λ_p	0.50 W m^{-1} K^{-1}

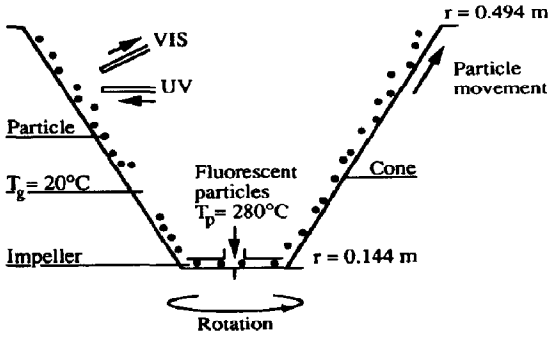

Fig. 2. Schematic representation of the cold flow facility.

Local particle velocity measurements

The local particle velocity has been obtained from shutter-controlled photographs of a part of the particle trajectory. With a video shutter time of 1 ms, the particle trajectories were visible as streaks of several mm length. Each recorded particle streak has a length which is proportional to the local particle velocity. The photographic technique has been applied by Wagenaar *et al.* (1994a) in his study of particle dynamics and gas-phase hydrodynamics in a rotating cone reactor.

Local particle temperature measurements

The local particle temperature has been measured with a fluoroptic particle temperature measurement technique described in more detail elsewhere (Wagenaar *et al.*, 1994b). This fluoroptic technique is based on the temperature dependence of the fluorescence spectrum produced by irradiating a certain phosphor with ultraviolet light. A phosphor with a colour shift from green to blue (with corresponding

temperature increase from 20 to 280°C) has been applied. This non-intrusive temperature measurement technique has been developed for non-contact measurement of the temperature of single particles with a diameter as small as 100 μm.

The fluoroptic set-up consists of a light source that generates the primary UV radiation. A quartz fibre cable guides the UV radiation to the detection spot; see Fig. 2. Fluorescent particles travel through this spot and upon illumination with UV light the particle swarm emits visible light (observable as a colour change). This colour change corresponds in a unique way to the mean temperature of the particle swarm. The visible light emitted by the particles is collected with a glass fibre cable and guided to optical filters that separate the colour signal into a blue and green component. The resulting optical signal is subsequently transformed into an electrical signal by photomultipliers that simultaneously amplify the electrical signal. Finally, the electrical signal is send to a data-aquisition unit for further processing. Figure 3 shows the main elements of the experimental temperature measurement technique.

The functional dependency which relates the measured green-to-blue intensity ratio to the particle temperature must be obtained by calibration. A sample of particles was placed on a heated surface with a temperature that could be varied from 20 to 300°C. The surface temperature was measured with a thermocouple. The sample was illuminated continuously which yielded the measured green-to-blue intensity ratio given in Fig. 4. As mentioned before, in systems of engineering interest the particles usually move through the illuminated spot which corresponds to non-stationary illumination. To simulate this effect, the UV-beam illuminating the particles was chopped by a disk with a narrow slit rotating at an appropriate frequency. The light pulses generated with this technique had a duration of approximately 1 ms. The results of these measurements are also shown in Fig. 4 from which a small dynamical effect is evident. This effect causes a maximum error of 10°C in temperature measurement.

3. LOCAL PARTICLE AND GAS-PHASE VELOCITY MEASUREMENTS

As mentioned in the Introduction the gas-to-particle heat transfer coefficient is dependent on the slip velocity between the particles and the gas phase. First results of the local gas-phase velocity measurements are presented. Secondly, results of the local particle velocities are presented. Calculation of the slip velocity between the particles and the gas phase can then be obtained by subtraction of the measured particle velocity and the gas-phase velocity. The spherical coordinate system, which is presented in Fig. 5, has been chosen as the natural base for representation of the velocity components in the cone.

Particles move along the rotating cone wall with a bouncing type of solids motion and exhibit a bouncing height which varies between 5 and 20 mm. The volumetric solids fraction has a value of 4×10^{-5} for a typical experiment (solids mass flow rate 5 g/s, bouncing height 15 mm and a solids residence time of 0.2 s). In this case, it was assumed that an undisturbed gas-phase velocity is permitted because the solids flow

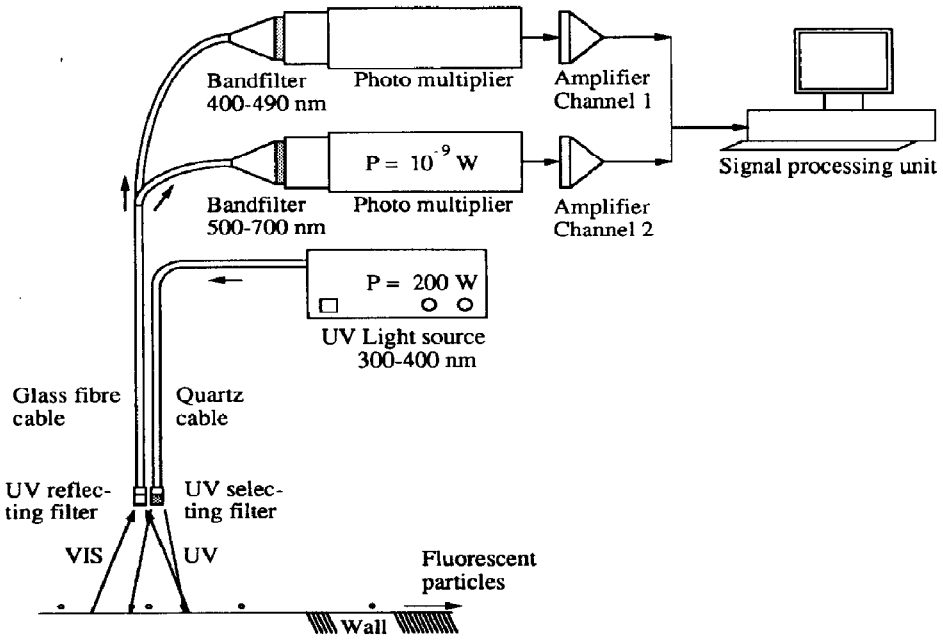

Fig. 3. The fluoroptic measurement system.

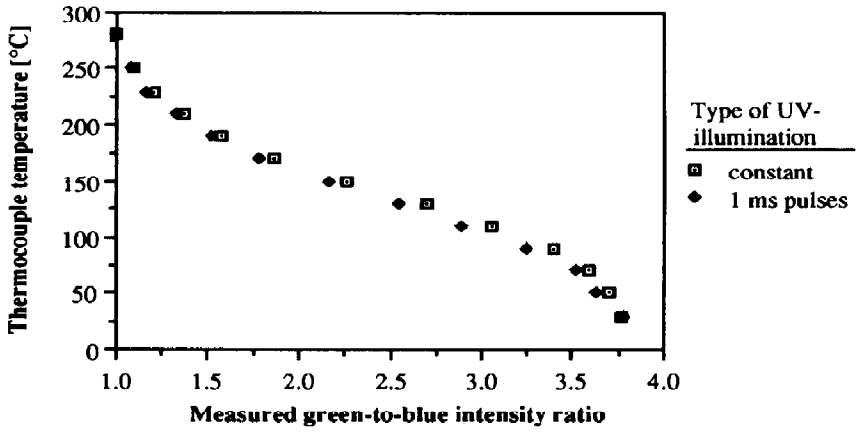

Fig. 4. The measured thermocouple temperature vs the measured green-to-blue intensity ratio, under various illumination conditions.

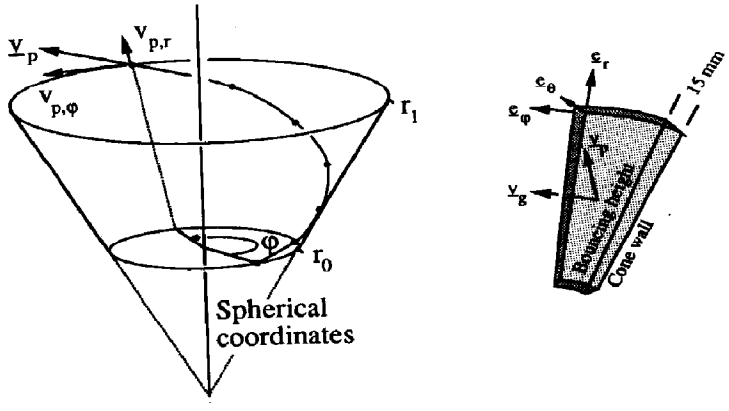

Fig. 5. The velocity components in spherical coordinates. A volumetric section of the cone wall is given in which the bouncing particles are confined.

is sufficiently dilute. To obtain some qualitative information regarding the flow behaviour of the gas phase inside the rotating cone reactor, some preliminary experiments were performed in which the motion of injected smoke was studied with the aid of a photographic technique. It was established that the rotational speed of the gas cloud in the core of the cone was approximately $\frac{1}{4}$ of the cone rotational speed. These smoke experiments also revealed the occurrence of swirls throughout the gas phase which supports the assumption of a fully developed turbulent flow at cone rotational frequencies above 7.5 Hz. Local gas-phase velocity measurements obtained with a hot wire anemometer were in good agreement with the qualitative smoke injection experiments. The angular velocity of the rotating gas cloud was measured at a distance of 3 mm from the cone wall and is presented in Fig. 6. This figure shows the ratio of the angular gas-phase velocity and the cone wall velocity as a function of the radial coordinate for several rotational frequencies of the cone. From this figure it can be observed that the aforementioned ratio is approximately constant.

Local particle velocity components have been measured using the aforementioned photographic technique. This technique yields the projection of the particle velocity on the conical surface which precludes the measurement of the velocity component normal to the cone wall. However, results from numerical simulations in which the particle position as a function of time has been calculated (Wagenaar *et al.*, 1994a) showed that the particle velocity component normal to the cone wall is small with respect to the radial and angular velocity components. Figure 7 shows the ratio of the radial particle velocity and the cone wall velocity as a function of the radial coordinate. In Fig. 8 the ratio of the angular particle velocity and the cone wall velocity as a function of the radial coordinate is shown. The declining trend in both figures indicates that the transfer of momentum to the particles is relatively small since the particles are not able to maintain a fraction of the cone wall velocity.

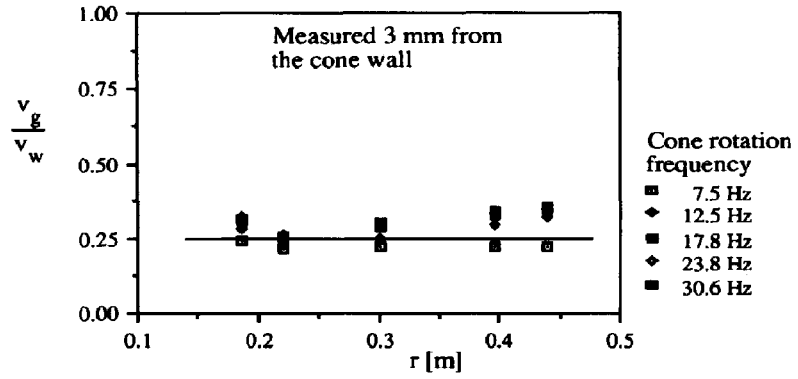

Fig. 6. The ratio between the angular gas-phase velocity and the cone wall velocity vs the radial coordinate.

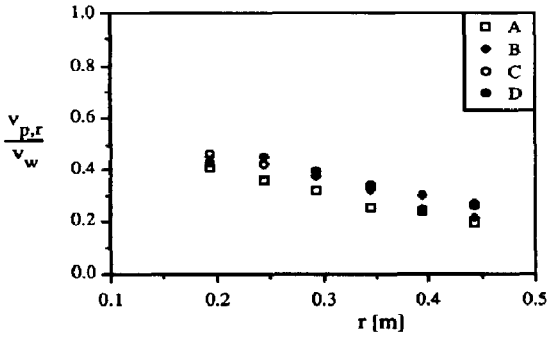

Fig. 7. The ratio between the radial particle velocity and the cone wall velocity vs the radial coordinate for various combinations of the particle diameter d_p and the cone rotational frequency n. (A) $n = 11.3$ Hz, $d_p = 155$ μm; (B) $n = 11.3$ Hz, $d_p = 280$ μm; (C) $n = 11.3$ Hz, $d_p = 425$ μm; (D) $n = 28.3$ Hz, $d_p = 280$ μm.

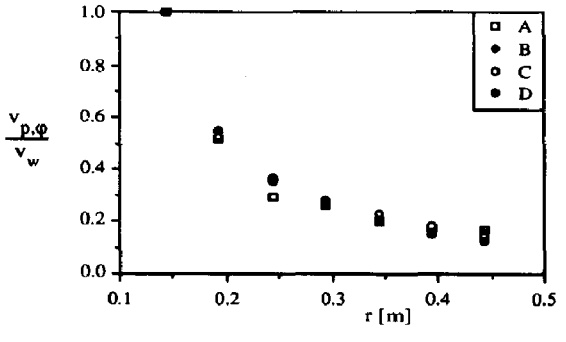

Fig. 8. The ratio between the angular particle velocity and the cone wall velocity vs the radial coordinate for various combinations of the particle diameter d_p and the cone rotational frequency n. (A) $n = 11.3$ Hz, $d_p = 155$ μm; (B) $n = 11.3$ Hz, $d_p = 280$ μm; (C) $n = 11.3$ Hz, $d_p = 425$ μm; (D) $n = 28.3$ Hz, $d_p = 280$ μm.

As indicated in these figures the measurements have been carried out for three different average particle diameters and two rotational frequencies of the cone.

The radial component of the slip velocity is equal to the radial particle velocity because the gas phase has a negligible radial velocity component as shown by hot wire anemometry. Figure 9 gives the radial velocity component of the particles as a function of the radial coordinate. From this figure a direct inspection of the radial particle velocity component is possible. However, the angular component of the velocity difference depends on both the angular gas-phase velocity and the angular particle velocity. Figure 10 shows the angular velocity component of the gas phase and the particle phase as a function of the radial coordinate. Note that the angular component of the slip velocity (i.e. $v_{p,\varphi} - v_{g,\varphi}$) is positive for $r < 0.3$ m and negative for $r > 0.3$ m. The intersection of both lines indicates the radial coordinate at which the angular component of both phases is similar.

The interpretation of the experimental data (i.e. determination of the average heat transfer coefficient along the particle trajectory) requires the definition of a trajectory averaged particle Reynolds number Re_p defined by

$$Re_p = \frac{|\mathbf{v}_p - \mathbf{v}_g|_{av}\, d_p}{\nu_g} \tag{2}$$

where $|\mathbf{v}_p - \mathbf{v}_g|_{av}$ represents the magnitude of the average slip velocity. This quantity has been determined following two different approaches which have been termed the "crude estimate approach" and the "application-based approach".

Crude estimate approach

In the crude estimate approach the average slip velocity has been obtained by computing the linear average of the velocity difference along the radial coordinate:

$$(\mathbf{v}_p - \mathbf{v}_g)_{av} = \frac{1}{\Delta r}\int_{r_0}^{r_1} (\mathbf{v}_p - \mathbf{v}_g)\,\mathrm{d}r. \tag{3}$$

For the evaluation of the integral on the right-hand side of eq. (3) the local velocity component of the gas phase and the particles in both radial and angular

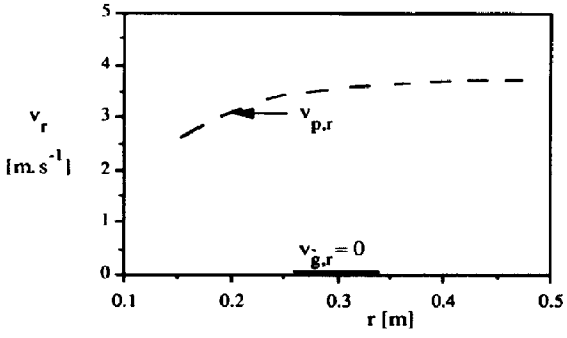

Fig. 9. The radial particle velocity as a function of the radial coordinate. The cone rotational frequency equals 11.3 Hz.

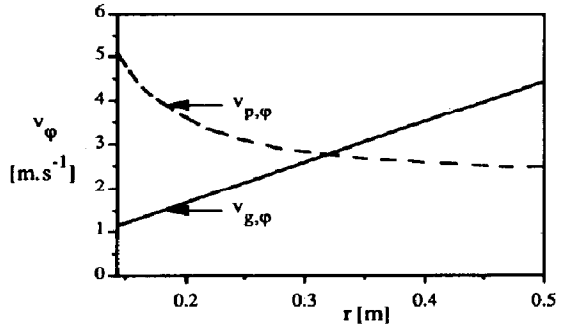

Fig. 10. The angular velocity components of the gas phase and the particles at a cone rotation frequency of 11.3 Hz.

directions are required. The radial component of the velocity difference between particles and gas phase depends only on the radial particle velocity, since the gas phase has a negligible radial velocity component. An advantage of the crude estimate approach, if applicable, is that transformation of the measurement data is not necessary which simplifies the interpretation of the averaged slip velocity. Here the velocity data of the gas phase and the particle phase, as presented in Figs 9 and 10, can be used to obtain an estimate of the average slip velocity.

Application-based approach

In the application-based approach a different averaging procedure of the local slip velocity has been used. This averaging procedure was motivated by inspection of the Ranz–Marshall equation for convective heat transfer to a single spherical particle:

$$Nu_p = \frac{\alpha_p d_p}{\lambda_g} = 2 + 0.6 Re_p^{0.50} Pr^{0.33}$$

$$= 2 + 0.6 \left(\frac{|\mathbf{v}_p - \mathbf{v}_g| d_p}{\nu_g} \right)^{0.50} \left(\frac{\nu_g}{a} \right)^{0.33}. \quad (4)$$

In the rotating cone the magnitude of the slip velocity $|\mathbf{v}_p - \mathbf{v}_g|$ is position-dependent which implies that a proper averaging procedure has to be performed in order to obtain the average heat transfer coefficient along the particle trajectory. From the Ranz–Marshall equation it can be seen that averaging along the particle trajectory corresponds to integrating the square root of the magnitude of the slip velocity along the particle trajectory. This leads to the conclusion that the average slip velocity should be computed on the basis of the following formulae:

$$|\mathbf{v}_p - \mathbf{v}_g|_{av}^{0.5} = \frac{1}{\tau} \int_0^\tau |\mathbf{v}_p - \mathbf{v}_g|^{0.5} \, dt \quad (5)$$

where τ denotes the particle residence time. Note that this expression differs from expression (3) which is based on a linear average.

Table 2 shows a comparison between the results obtained by the aforementioned approaches. From this table it can be concluded that both approaches produce very similar quantitative results. If the crude estimate approach is used in combination with the velocity data from Figs 9 and 10, it can be concluded that the slip velocity is dominated by the radial particle velocity component.

4. LOCAL PARTICLE TEMPERATURE MEASUREMENTS

Local particle temperatures have been measured to provide the necessary data for calculating the average particle Nusselt number. Two examples of such measurements are given in Figs 11 and 12 which show the measured particle temperature as a function of the radial coordinate r. In addition to the radial coordinate, the particle travelling time is given in each figure. This time coordinate is obtained by evaluating the integral on the right-hand side of the following equation:

$$t_p = \int_{r_0}^{r} \frac{dr}{v_{p,r}}. \quad (6)$$

For the interpretation of the experimental data it is convenient to introduce the following dimensionless

Table 2. Average velocity difference between particle and gas phase

	Crude approach			Application-based approach
n (Hz)	$(v_p - v_g)_{r,av}$	$(v_p - v_g)_{\varphi,av}$	$\|\mathbf{v}_p - \mathbf{v}_g\|_{av}$	$\|\mathbf{v}_p - \mathbf{v}_g\|_{av}$
11.3	3.5	1.5	3.8	4.0
28.3	10	4	11	10.3

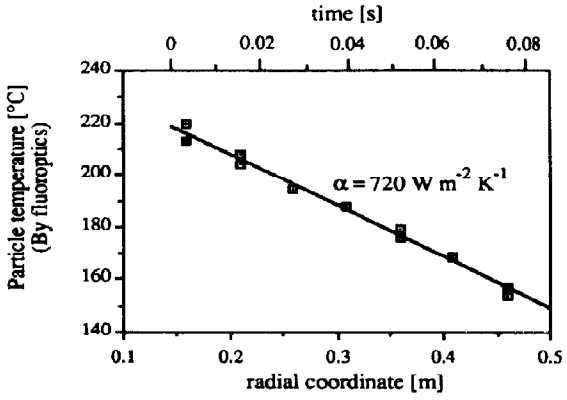

Fig. 11. The measured particle temperature as a function of the radial coordinate in the cone. Cone rotational frequency 11.3 Hz and the average particle diameter equals 425 μm.

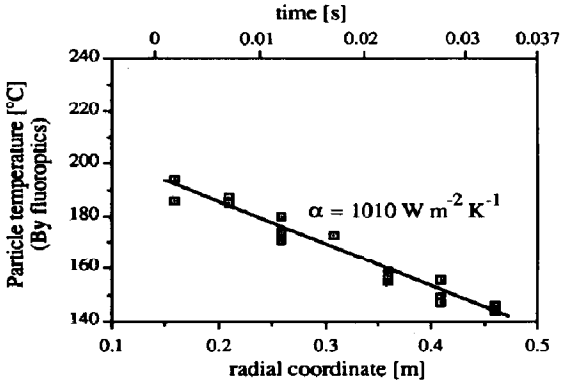

Fig. 12. The measured particle temperature as a function of the radial coordinate in the cone. Cone rotational frequency 28.3 Hz and the average particle diameter equals 280 μm.

thermal driving force Y_p:

$$Y_p = \frac{T_p - T_g}{T_{p,\text{feed}} - T_g} \tag{7}$$

in which T_p denotes the average particle temperature and T_g the bulk temperature of the gas phase. Temperature measurements of the gas phase in the vicinity of the cone wall showed that the gas-phase temperature was equal to the room temperature (30°C). It should be stressed that the temperatures which are obtained from the fluoroptic technique are the particle surface temperatures. The difference between the average particle temperature T_p and the particle surface temperature can be neglected in case the Biot number Bi is sufficiently small. The Biot number is defined as the ratio of the particle internal heat transfer resistance and the external heat transfer resistance and can be used to estimate whether temperature gradients inside the particle are present. This Biot

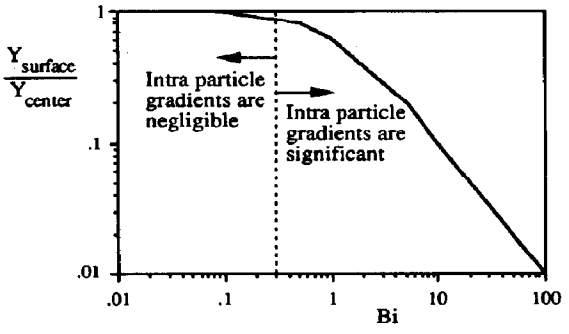

Fig. 13. The maximum ratio of the thermal driving force at the particle surface and the thermal driving force in the centre of the spherical particle as a function of the Biot number.

number is defined as

$$Bi = \frac{\alpha_p R_p}{\lambda_p}. \tag{8}$$

If a hot particle is suddenly exposed to a cold medium, the ratio of the thermal driving force at the particle surface and the thermal driving force at the particle centre will be at a maximum at a certain point in time. This maximum ratio of the thermal driving forces is presented in Fig. 13 as a function of the Biot number. From this figure it can be concluded that intraparticle temperature gradients can be neglected if the value of the particle Biot number is smaller than 0.3. This is especially important because the temperature indicating phosphor particles are dispersed in a transparent glasseous matrix and are visible even below the particle surface. In the case of small Biot numbers a uniform particle temperature can be assumed and the change of particle temperature as a function of time is given by eq. (9):

$$Y_p = \exp\left(-\frac{6\alpha_p t}{\rho_p C_p d_p}\right) \tag{9}$$

where $\rho_p C_p$ represents the volumetric heat capacity of the fluorescent particles. The gas-to-particle heat transfer coefficient α_p has been calculated from a best fit of eq. (9) with respect to the experimentally obtained dimensionless particle temperature Y_p as a function of time t. Values of this gas-to-particle heat transfer coefficient are given in Table 3 together with the values of the Biot number. Because the Biot numbers given in Table 3 are smaller than 0.3, intraparticle temperature gradients could indeed be neglected.

5. A RELATIONSHIP BETWEEN THE REYNOLDS, NUSSELT AND PRANDTL NUMBER

Heating or cooling of particles in a convective gas flow can in principle be described on the basis of the conservation equations of mass, momentum and thermal energy (Bird *et al.*, 1960). By specifying appropriate initial and boundary conditions these transport equations can be solved to yield the velocity and

Table 3. The external particle heat transfer coefficient for different experimental conditions

n (Hz)	d_p (μm)	α_p	Bi
11.3	155	280	0.04
11.3	280	490	0.14
11.3	425	660	0.28
28.3	155	930	0.14
28.3	280	1030	0.29

temperature distributions. From these distributions the average gas-to-particle heat transfer coefficient can in principle be calculated. However, due to mathematical complexity the aforementioned approach is normally not followed; instead, an empirical approach involving dimensionless groups is used. By transforming the transport equations of mass, momentum and thermal energy in dimensionless form, and applying the Buckingham Π-theorem (Buckingham, 1914), it can be shown that the following functional dependency exists between the particle Nusselt number Nu_p, the particle Reynolds number Re_p and the Prandtl number Pr:

$$F(Re_p, Nu_p, Pr) = 0 \tag{10}$$

where

$$Nu_p = \frac{\alpha_p d_p}{\lambda_g} \tag{11}$$

$$Re_p = \frac{|\mathbf{v}_p - \mathbf{v}_g|_{av}\, d_p}{\nu_g} \tag{12}$$

and

$$Pr = \frac{\nu_g}{a}. \tag{13}$$

In eq. (10), Re_p and Nu_p represent, respectively, the average particle Reynolds number and the average particle Nusselt number. In Table 4 the dimensionless groups corresponding to the experimental data of Tables 2 and 3 are shown. Since air has been used in each experiment as the coolant the Prandtl number is a constant (approximately 0.71 for air at 30°C).

Experiments involving convective heat transfer to non-rotating spheres fixed in space were performed among others by Ranz and Marshall (1952). In their study, spheres were exposed to a convective fluidum flow with negligible turbulence intensity. The relationship between the particle Nusselt number Nu_p, the particle Reynolds number Re_p and Prandtl number Pr obtained from their experiments is given by

$$Nu_p = 2 + 0.6 Re_t^{0.5}\, Pr^{0.33}. \tag{14}$$

Because the experimental conditions of the heat transfer study performed by Ranz and Marshall resemble the experimental conditions of the work reported in this paper, a closer comparison between the results of both studies has been made. In Fig. 14 the experimentally determined average particle Nusselt number is shown as a function of the average particle Reynolds number. For reference purposes the Ranz–Marshall correlation is included in this figure.

6. DISCUSSION

From Fig. 14 it can be seen that the Nusselt numbers obtained in the present work can only approximately be described by the Ranz–Marshall correlation. This deviation is most probably due to differences between the experimental set-up used by Ranz and Marshall and the experimental set-up used in this work. Table 5 shows some important factors influencing gas-to-particle heat transfer in a gas–solid system.

The possible rotation of particles inside the rotating cone reactor constitutes a major difference with respect to the hydrodynamic conditions prevailing in the heat transfer study of Ranz and Marshall. The occurrence of particle rotation is most likely due to the impact of irregular-shaped particles on the rotating cone wall. This phenomenon has also been observed by Matsumoto and Saito (1970). To estimate the magnitude of the convective heat transfer due to particle rotation subsequently, a simple model will be presented which describes the decay of the particle rotation frequency as a function of time. In addition, some literature correlations will be presented which give the Nusselt numbers for heat transfer from a rotating sphere to quiescent air. Finally, a general method due to Churchill (1982) will be presented with which the heat transfer contributions originating from different hydrodynamic mechanisms can be combined to obtain the total heat transfer coefficient.

To obtain a relation describing the decay of the particle rotational frequency ω the torque balance on a particle serves as a starting point:

$$I \frac{d\omega}{dt} = -\tau \tag{15}$$

where I represents the moment of inertia and τ the torque acting on the body under consideration. For

Table 4. Dimensionless representation of the experimental data

n (Hz)	d_p (μm)	$\lvert\mathbf{v}_p - \mathbf{v}_g\rvert_{av}$	Re_p	α_p	Nu_p
11.3	155	4.0	45	280	1.7
11.3	280	4.0	81	490	5.3
11.3	425	4.0	123	660	10.9
28.3	155	10.3	115	930	5.6
28.3	280	10.3	208	1030	10.9

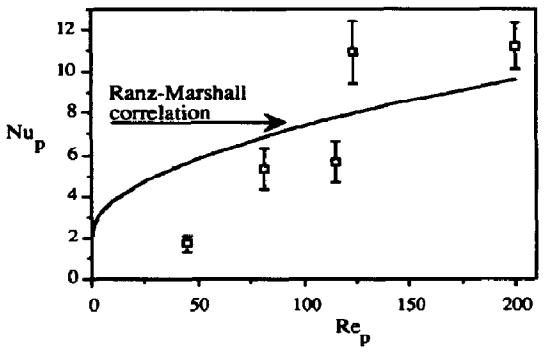

Fig. 14. The particle Nusselt numbers vs the particle Reynolds number. The data points correspond to the experimentally determined values. The curve corresponds to the Ranz–Marshall correlation.

a spherical body the moment of inertia I is given by eq. (16), whereas the torque acting on a rotating sphere is given by eq. (17):

$$I = \tfrac{2}{5} m_p R_p^2 \tag{16}$$

$$\tau = \xi_t \tfrac{1}{2} \rho_g R_p^5 \omega^2. \tag{17}$$

The torque coefficient ξ_t depends on the Reynolds number for a rotating sphere Re_ω as given by Sawatzki (1970):

$$\xi_t = \frac{16\pi}{Re_\omega}, \quad Re_\omega < 26.25 \tag{18}$$

$$\xi_t = \frac{16\pi}{3Re_\omega} + \frac{6.54}{\sqrt{Re_\omega}}, \quad 26.25 < Re_\omega < 12{,}000 \tag{19}$$

$$\xi_t = 0.4 Re_\omega^{-0.2} \quad Re_\omega > 12{,}000 \tag{20}$$

where the Reynolds number for a rotating sphere is given by

$$Re_\omega = \frac{\omega R_p^2}{\nu_g}. \tag{21}$$

If eqs (15)–(18) are combined and solved, the following solution for particle rotation frequency as a function of time is obtained:

$$\frac{\omega}{\omega_0} = \exp\left(-15 \frac{\nu_g t}{R_p^2} \frac{\rho_g}{\rho_p} \right), \qquad Re_\omega < 26.25 \tag{22}$$

where ω_0 represents the initial particle rotation frequency. It should be borne in mind that eq. (22) is valid only in the laminar regime (i.e. $Re_\omega < 26$). The characteristic time t in equation (22) follows from the elapsed time between two successive particle collisions with the cone wall. This time has been obtained from a detailed hydrodynamic model presented elsewhere (Wagenaar *et al.* 1994a) and equals approximately 0.05 s. When it is assumed that during each wall collision the particle attains an initial rotational frequency ω_0 then the decay of this frequency during the subsequent free flight motion of the particle can be computed from eq. (22). Rotation of particles in free flight, induced by particle–wall collisions, has been observed experimentally by Matsumoto and Saito (1970). The smallest particles lose their rotation easily due to viscous damping as can be seen from an inspection of eq. (22). For the smallest particles used in this study ($d_p = 155\ \mu$m) the particle rotation frequency which is initiated by a particle–wall collision only reduces by 50% after 0.1 s which indicates that continuous particle rotation occurred in the experiments.

Heat transfer from a rotating sphere to quiescent air has been studied by Tieng and Yan (1993), Farouk (1985) and Kreith *et al.* (1963). Kreith *et al.* obtained a correlation which is given by eq. (23). For the purpose of reference to the original work we retained the original formulation. The Ranz–Marshall equation is also given below:

$$Nu_p = 2 + A\, Re_r^{0.50} Pr^{0.33}, \quad A = 0.43, \quad Re_p = 0, \quad 0 < Re_r < 5 \times 10^4, \quad 0.72 < Pr < 217 \tag{23}$$

$$Nu_p = 2 + B\, Re_p^{0.50} Pr^{0.33}, \quad B = 0.60, \; Re_r = 0, \quad 0 < Re_p < 3 \times 10^4, \quad 0.71 < Pr < 380. \tag{24}$$

The fluidum-to-sphere mass transfer in the case of a rotating sphere exposed to a translational fluid flow has been studied by Furuta *et al.* (1975) and Noordsij and Rotte (1968). Furuta *et al.* positioned the sphere rotation axis parallel to the fluid flow and observed that the rotational and translational mass transfer assisted each other. Noordsij and Rotte placed the sphere rotation axis perpendicular to fluid flow and observed that the mass transfer by rotation counteracted the mass transfer by translation. On the basis of intuition this is unexpected behaviour since one would presume that any rotation would increase the mass transfer coefficient due to enhanced convective mass transport. However, in practice this is not always the case as is evident from the results reported by Noordsij and Rotte. It is likely that the magnitude of the local gas-phase velocity in the downwind vicinity of the particle surface is diminished due to particle rotation. In addition the thermal boundary layer

Table 5. Factors influencing the gas-to-particle heat transfer

Factor	This study	Ranz and Marshall
Dominant mode of the gas-to-particle heat transfer	Convective	Convective
Body environment	Free body	Free body
Body shape	Irregular	Sphere
Rotation mode	Free rotation	Non-rotating

thickness is expected to be larger at the upwind side of the particle because of the prolonged contact time of fluid elements by rotation of the particle. It is speculated that this phenomenon is not captured in our measurements of the local gas-phase velocity. From the experimental results obtained by Noordsij and Rotte, a minimum in the value of the fluid-to-sphere mass transfer coefficient was observed if the value of the sphere rotational Reynolds Re_r number was approximately equal to the value of the sphere translational Reynolds number Re_p.

Churchill (1982) proposed a general method to combine the heat/mass transfer contributions originating from two different hydrodynamic mechanisms. In the case of assisting mass transfer from rotation and translation, as observed by Furuta *et al.* (1975), the combination yields

$$Sh_p - 2 = (A^3\, Re_r^{1.5}\, Sc + B^3\, Re_r^{1.5}\, Sc)^{0.33}. \quad (25)$$

Coefficients A and B originate from eqs (23) and (24). Furuta *et al.* derived this equation on a more fundamental basis. In the case of counteracting mass transfer from rotation and translation, as observed by Noordsij and Rotte, the combination yields

$$Sh_p - 2 = |A^3\, Re_r^{1.5}\, Sc - B^3\, Re_r^{1.5}\, Sc|^{0.33}. \quad (26)$$

Chilton and Colburn (1934) showed that heat and mass transfer are mathematically analogous at low heat/mass transfer rates. For an inspection of the analogy conditions, the reader is referred to their work. As a consequence of the Chilton–Colburn analogy, the mass transfer studies of Furuta *et al.* (1975) and Noordsij and Rotte (1968) can also be applied to describe the flow of heat to rotating spheres in a convective flow. Then the particle Sherwood number Sh_p is replaced by the particle Nusselt number Nu_p and the Schmidt number Sc is replaced by the Prandtl number Pr.

The overall effect of free particle rotation on the transfer of heat to particles is uncertain, since it is related to the direction of the gas flow and the direction of the particle rotation axis. Due to the random nature of the collision of a roughly shaped particle with a smooth wall, the particle will rotate around its three principle rotation axes. Therefore, gas-to-particle heat transfer probably contains the effects of both assisting and counteracting heat transfer simultaneously which will give rise to scattering of the experimentally observed gas-to-particle heat transfer coefficients in the geometry considered in the present study.

7. CONCLUSIONS

Experimental results obtained in the rotating cone reactor showed that the correlation of the value of the particle Reynolds number with the value of the particle Nusselt number can only be described approximately by the Ranz–Marshall correlation.

Rotation of the particles was present in the rotating cone reactor. Heat transfer effects due to the rotation of the particles is probably damped by the assisting and counteracting heat transfer mechanisms when particles are rotating in a convective flow.

It was shown that the experimental scatter in the measured gas-to-particle heat transfer coefficient is most probably caused by rotation of the freely flowing particles.

Calculation of the average velocity difference between the gas phase and the particulate phase can be based on a crude approximation and an application-based method. In case of the experiments, in the rotating cone reactor, both methods gave a similar velocity difference.

Acknowledgements—We thank M. Meijer and R. Meijer for their contributions to the experimental work. We also acknowledge the representatives of the EEC Joule program and the Dutch Novem, who provided financial grants which enabled this research to take place.

NOTATION

a	thermal diffusivity, $m^2\,s^{-1}$
A	surface, m^2
Bi	Biot number ($= \alpha R_p/\lambda_p$), dimensionless
C_p	heat capacity, $J\,kg^{-1}\,K^{-1}$
d_p	particle diameter, m
D	diffusion coefficient, $m^2\,s^{-1}$
I	moment of inertia, $kg\,m^2$
m	mass, kg
n	cone rotational frequency, s^{-1}
Nu_p	particle Nusselt number ($= \alpha\, d_p/\lambda_g$), dimensionless
Pr	Prandtl number ($= \eta_g\, C_g/\lambda_g$), dimensionless
Q''	heat flux, $W\,m^{-2}$
R_p	particle radius, m
Re_p	translational particle Reynolds number ($= v_g d_p/v_g$), dimensionless
Re_r	rotational particle Reynolds number ($= \omega\, d_p^2/v_g$), dimensionless
Re_ω	rotational particle Reynolds number ($= \omega R_p^2/v_g$), dimensionless
Sc	Schmidt number ($= v_g/D$)
t	time, s
T	temperature, K
Y	dimensionless thermal driving force

Greek letters

α	heat transfer coefficient, $W\,m^{-2}\,K^{-1}$
η	viscosity, Pa s
λ	thermal conductivity, $W\,m^{-1}\,K^{-1}$
ν	kinematic viscosity, $m^2\,s^{-1}$
ξ_t	Torque coefficient, dimensionless
ρ	density, $kg\,m^{-3}$
τ	torque, $kg\,m^2\,s^{-2}$
ω	angular velocity, $rad\,s^{-1}$

Subscripts

av	average
p	particle
g	gas
0	initial.

REFERENCES

Bird, R. B., Stewart, W. E. and Lightfoot, E. N., 1960, *Transport Phenomena*. Wiley, New York.

Buckingham, E., 1914, On physically similar systems; illustrations of the use of dimensional equations. *Phys. Rev.* **4**, 345.

Chilton, T. H. and Colburn, A. P., 1934, Mass transfer (absorption) coefficients—prediction from data on heat transfer and fluid friction. *Ind. Engng Chem.* **26**, 1183.

Churchill, S. W., 1982, The development of theoretically based correlations for heat and mass transfer. *Proceedings of the 1st Latin-American Conference on Heat and Mass Transfer*, La Plata, Argentina, p. 207.

Farouk, B., 1985, Mixed convective flows around a slowly rotating isothermal sphere. *ASME J. Heat Transfer* **107**, 431.

Furuta, T., Jimbo, T., Okazaki, M. and Toei, R., 1975, Mass transfer to a rotating sphere in an axial stream. *J. Chem. Engng Jpn* **8**, 456.

Igarashi, T., 1985, Heat transfer from a square prism to an air stream. *Int. J. Heat Mass Transfer*, **28**, 175.

Kreith, F., Roberts, L. G., Sullivan, J. A. and Sinha, S. N., 1963, Convection heat transfer and flow phenomena of rotating spheres. *Int. J. Heat Mass Transfer* **6**, 881.

Matsumoto, S. and Saito, S., 1970, On the mechanism of suspension of particles in horizontal pneumatic conveying: Monte Carlo simulation based on the irregular bouncing model. *J. Chem. Engng Jpn* **3**, 83.

Noordsij, P. and Rotte, J. W., 1968, Mass transfer coefficients for a simultaneously rotating and translating sphere. *Chem. Engng Sci.* **23**, 657.

Ranz, W. E. and Marshall, W. R., 1952, Evaporation from drops, Part 2. *Chem. Engng Progress* **48**, 173.

Sawatzki O., 1970, Das Stromungsfeld um eine rotierende Kugel. *Acta Mech.* **9**, 159–214.

Tieng, S. M. and Yan, A. C., 1993, Experimental investigation on convective heat transfer of heating spinning sphere. *Int. J. Heat Mass Transfer* **36**, 599.

Wagenaar, B. M., Kuipers, J. A. M. and Van Swaaij, W. P. M., 1994a, Particle dynamics and gas phase hydrodynamics in a rotating cone reactor. *Chem. Engng Sci.* **49**, 927.

Wagenaar, B. M., Meijer, R., Kuipers, J. A. M. and Van Swaaij, W. P. M., 1994b, A novel method for non-contact measurement of particle temperatures. *A.I.Ch.E. J.* (accepted for publication).